Journal of Marine Research, 76, 23–46, 2018

Why is the ocean surface slightly warmer than the atmosphere?

by Lakshika Girihagama[1,2,4] and Doron Nof[1,3]

ABSTRACT

How much warmer is the ocean surface than the atmosphere directly above it? The present study offers a means to quantify this temperature difference using a conceptual nonlinear one-dimensional global energy balance coupled ocean–atmosphere model ("*Aqua Planet*"). The significance of our idealized model, which is of intermediate complexity, is its ability to obtain an analytical solution for the global average temperatures. Our analytical model results show that, for the present climate, predicted global mean ocean temperature is 291.1 K whereas surface atmospheric temperature above the ocean surface is 287.4 K. Thus, the modeled surface ocean is 3.7 K warmer than the atmosphere above it. Temporal perturbation of the global mean solution obtained for "*Aqua Planet*" showed a stable system. Oscillation amplitude of the atmospheric temperature anomaly is greater in magnitude than those found in the ocean. There is a phase shift (a lag in the ocean), which is caused by oceanic thermal inertia. Climate feedbacks due to selected climate parameters such as incoming radiation, cloud cover, and CO_2 are discussed. Warming obtained with our model compares well with Intergovernmental Panel on Climate Change's (IPCC) estimations. Application of our model to local regions illuminates the importance of evaporative cooling in determining derived air–sea temperature offsets, where an increase in the latter increases the systems overall sensitivity to evaporative cooling.

Keywords: Temperature difference, ocean–atmosphere interaction, conceptual climate models

1. Introduction

How heat transfer processes shape the atmospheric and oceanic temperatures is a fundamental question for climate scientists because the temperature difference between the ocean the atmosphere is essential to study the climate variability and its feedbacks. In general, one would expect the ocean to be warmer than the overlying atmosphere because approximately 50% of incoming solar radiation is absorbed by the ocean, whereas less than 20% is absorbed in the atmosphere, which is largely heated from below. Therefore, one can

1. Geophysical Fluid Dynamics Institute, Florida State University, Tallahassee, Florida, USA.
2. Corresponding author: ***e-mail: lakshika.rwrh@utoronto.ca***
3. Department of Earth, Ocean, and Atmospheric Science Department, Florida State University, Tallahassee, Florida, USA.
4. Department of Physical and Environmental Sciences, University of Toronto Scarborough, Toronto, Ontario, Canada.

raise the question, "on a global scale, how much warmer is the ocean than the atmosphere above it?" This is important because the direction of the heat flow at the air–sea interface is dependent on this difference. However, to our knowledge there has been little attention given to understanding the air–sea temperature difference (offset) and, hence, few literatures have addressed this problem. Although direct measurement of global sea surface temperature (SST) is available through satellite data, the estimation of surface air temperature is acquired through indirect methods. For instance, Liu (1988) extracted SST from satellites but estimated the surface air temperature using constant specific humidity ($\sim$80%). In another example, Singh, Kishtawal, and Joshi (2005) used a genetic algorithm to determine monthly global mean SST and in situ measured surface air temperature and found a natural variance of the observed offset as 1.7°C, 1.0°C, and 0.7°C for higher northern latitudes, southern higher latitudes, and the tropics, respectively. Their study showed that, after removing systematic biases, the global air–sea surface temperature difference is 0.40 ± 0.11°C. Kara, Hurlburt, and Loh (2007) showed the global climatological air–sea temperature difference as 0.94°C and 0.64°C using Comprehensive Ocean–Atmosphere Data Set (COADS) and the European Centre for Medium-range Weather Forecasts (ECMWF) 40-year reanalysis (ERA-40) data, respectively. Their study concluded that the seasonal variability of the air–sea surface temperature offset is mainly driven by the variability in net radiation at the surface. Using detailed measurements from 1938, Dietrich (1963) also showed the ocean to be 0.8°C warmer than the atmosphere. However, the above estimations are purely based on observations and lack the theoretical understanding of setting the aforementioned air–sea temperature offset. Thus, we used an idealized, one-dimensional, nonlinear, coupled ocean–atmosphere model with an intermediate complexity to those discussed in classic energy balance models (e.g., Budyko 1969; Sellers 1969) to improve our theoretical understanding of the role that coupling between atmospheric dynamics and oceanic mixed-layer thermodynamics plays in setting the global mean air–sea temperature difference.

Over the past decades, there have been various theoretical and observational studies examining climate variability—on time scales longer than intraseasonal—in part because of the availability of large amounts of data, as well as the development of state of the art numerical models. As a result, a variety of climate models have been developed, ranging in complexity from simple one-dimensional models that consider only global averages to complex three-dimensional general circulation models (GCMs). The simplest model that described the planet's temperature assumed a black-body radiation where the planet's shortwave radiation is balanced by the outgoing long-wave radiation (see the review in North and Kim 2017). Classic simple energy balance climate models (e.g., Budyko 1969; Sellers 1969) discussed the effects of transport and ice–albedo effect where the entire climate is defined as a single temperature. The main difference between the black-body radiation and Budyko–Sellers-type simple energy balance models was the linear parameterization of long-wave radiation. North (1975), who used a radiative balance climate model similar to Budyko–Sellers but with an additional diffusive heat transport, discussed the analytical solution to Budyko–Sellers-type models. All of the above classic models, however, viewed

the ocean and atmosphere as a single system and, thus, lack the ability to explain the role of coupling between them. The first attempt at obtaining a two-layer energy balance model and the first heat budget analysis was proposed by Dines (1917). In his model the surface and the atmosphere were coupled through surface heat fluxes. The utility of Dines-type two–layer models was later examined by Kramm and Dlugi (2010) and Link and Lüdecke (2011), where both used sensible and latent heat flux estimates from Trenberth, Fasullo, and Kiehl (2009)'s budget analysis to incorporate the present climate. Readers may refer to Kramm and Dlugi (2010; 2011) and Link and Lüdecke (2011) for a detailed discussion of global energy balance models.

Air–sea *numerical coupling* was first introduced in the late 1960s and early 1970s (Manabe and Bryan 1969; Bryan, Manabe, and Pacanowski 1975; Manabe, Bryan, and Spelman 1975). In these ocean–atmospheric general circulation models, the fixed boundary condition provided by a slab ocean (uncoupled) is removed, as well as the negative feedback produced by it. Later, coupled GCMs were improved to include anthropogenic influences on climate (e.g., Gates et al. 1985; Schlesinger et al. 1985; Sperber et al. 1987; Bryan et al., 1988; Manabe and Stouffer, 1988; Washington and Meehl 1989; Stouffer et al. 1989; Manabe et al., 1990; Cubaschet al. 1992; Manabe et al., 1992). A wide range of coupled models have been used over the past decades to help resolve climate issues. Complex coupled GCMs provide a more accurate climate signal; however, they need large computational resources to produce results. Energy balance models with a simpler representation of physical and thermodynamical processes than GCMs, on the other hand, require less computational resources and are useful tool for studying feedbacks, sensitivities, and interactions within the climate system.

Our aim is to theoretically predict an analytical solution for temperatures in both the ocean and the atmosphere with a coupled climate model in a simple setting. Thus, we computed the ocean and atmospheric temperatures analytically using a nonlinear, global, coupled ocean–atmosphere model. Our conceptual climate model represents an "*Aqua Planet*" (Fig. 1), where planet Earth is assumed to be a box filled with water and is in equilibrium with the overlying mixed atmospheric box. At the global mean state, the model boundaries are assumed to be closed where averaging of lateral heat becomes zero in both mediums. Any communication between the ocean and atmosphere occurs via surface heat fluxes. At the top of the atmosphere, it receives shortwave radiation and reemits a portion of that radiation back to space through long-wave radiation. At the bottom of the atmosphere, it receives heat released by the ocean surface. All the heat transfer processes are parameterized using the sea surface water temperature and the surface atmospheric temperature. We acquired analytical solutions for this highly nonlinear coupled ocean–atmosphere system. To complete the discussion of climate variability and its feedbacks, we discussed our conceptual model responses to variability in selected climate parameters such as incoming radiation, cloud cover, and CO_2. We also complemented the model responses to climate variability by comparing its results with recent Intergovernmental Panel on Climate Change (IPCC) estimates. Further, we analyzed the stability of the mean solution by introducing a temporal

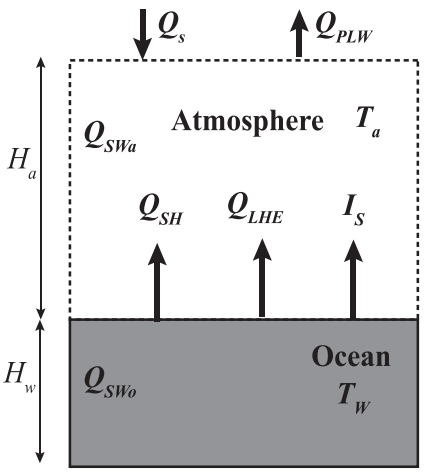

Figure 1. Illustration of the conceptual air–sea coupled global model ("*Aqua Planet*"), a one-dimensional box in which the mixed oceanic layer is physically in contact with the uniformly mixed atmospheric layer above it. Q_s is net solar radiation at the top of the atmosphere; Q_{SW} is absorbed shortwave radiation and H is scale height, where subscripts "a" and "w" refer to the atmosphere and ocean, respectively; Q_{PLW} is net long-wave flux out into space; Q_{LHE} is latent heat released at the surface due to evaporation; and Q_{SH} is surface sensible heat loss to the atmosphere.

perturbation. Initially, we looked for a homogenous system and assumed that temporal perturbation of shortwave radiation is insignificant. Later, temporal variation of shortwave radiation (annual variation) is included to understand the magnitudes of anomalous atmospheric temperature and surface water temperature fluctuations. Finally, we applied our model to marginal seas (e.g., Dead Sea, Caspian Sea, Mediterranean Sea, Red Sea, and Black Sea), at the equator (10 S–10 N), in the subtropics (10 N–40 N), and at higher northern latitudes (40 N–60 N). This illustrates regional variations of the air–sea temperature offset as compared with the global solution. We discussed the importance of the ratio of local-to-global temperature offset in determining the local evaporative cooling.

Organization of the remainder of this manuscript is as follows: Section 2 presents a detailed description of the coupled ocean–atmosphere model. Section 2a explains the governing thermodynamic equations and Section 2b explains the parameterization of individual heating components. Resulting equations are algebraic; however, their nonlinearity makes the system analytically unsolvable. Thus, in section 3, we used an iterative solution, for which we assumed a known temperature and allow the error to converge to zero. Results are discussed in section 4, in which section 4a discusses the mean state and section 4b presents the feedbacks due to variability in climate parameters, such as incoming radiation, cloud cover, and CO_2. Section 4c discusses the stability of the mean state to temporal perturbations where we assumed a homogenous system. Temporal perturbation of incoming radiation (annual solar cycle) generates a nonhomogenous linear system of equations. The

solution of this system is used to understand the magnitudes of anomalous atmospheric temperature and surface water temperature fluctuations in relation to seasonal radiation changes. In section 4d, we discuss application of our model to marginal seas, tropics, subtropics, and northern higher latitudes. Finally, a summery and conclusion is presented in section 5.

2. Model

a. Thermodynamic equations for the coupled ocean–atmosphere model

We used a one-dimensional coupled ocean–atmosphere model in which the mixed oceanic surface layer is physically in contact with the uniformly mixed atmospheric layer above it ("*Aqua Planet*"). The model contains two independent variables: atmospheric surface temperature (T_a) and water temperature (T_w). The interaction between the ocean and the atmosphere is implemented through surface heat fluxes (Fig. 1). Further, we assumed any changes due to surface areas in both mediums are insignificant in the "*Aqua Planet*" model. The atmospheric heat budget is given by

$$\rho_a H_a C p_a \frac{\partial T_a}{\partial t} = Q_{SW_a} + Q_{SH} + I_s - Q_{PLW} + Q_{LHE}, \tag{1}$$

(e.g., Rasool and Schneider 1971; Sellers 1974; Jentsch 1991; Weaver et al. 2001) where, ρ is the constant density, H is the constant scale height, Cp_a is the specific heat capacity at constant pressure, T is the temperature, Q_{SW_a} is the absorbed atmospheric shortwave radiation, Q_{SH} is the sensible heat released at the sea surface, I_s is the net long-wave flux released at the sea surface to the atmosphere, Q_{PLW} is the net long-wave radiation escaping into space, and Q_{LHE} is the latent heat due to evaporation. The subscript "a" refers to the atmosphere.

The oceanic heat budget is given as

$$\rho_w H_w C p_w \frac{\partial T_w}{\partial t} = Q_{SW_o} - Q_{SH} - I_s - Q_{LHE}, \tag{2}$$

where Q_{SW_o} is absorbed oceanic shortwave radiation and the subscript "w" refers to the ocean surface.

b. Parameterization of heating components

Heating components found on the right-hand side of Eqs. (1) and (2) are parametrized below. All parameterizations are defined as functions of modeled surface atmospheric (T_a) and water (T_w) temperatures.

i. Solar radiation. Net solar heating in the atmospheric column is given as

$$Q_{SW_a} = Q_S \left\{(1 - A_c)\left[A_b + T_r \alpha A_b/\left(1 - \alpha R_f\right)\right] + A_c\left[A_b^c + T_r^c \alpha A_b^c/\left(1 - \alpha R_f^c\right)\right]\right\} \tag{3}$$

(e.g., Shell and Somerville 2005; Wang et al. 2004) where α is surface albedo, R_f is reflectivity, A_b is absorptivity, T_r is transmissivity of the atmosphere, such that $A_b + R_f + T_r = 1$ and $A_b^c + R_f^c + T_r^c = 1$, A_c is cloud cover and Q_S is average global incoming solar radiation at the top of the atmosphere. The subscript "a" and the superscript "c" refer to the atmosphere and a cloudy sky, respectively. Optical properties of the atmosphere for a clear and cloudy sky are given in Wang et al. 2004. Because of the zero degrees of freedom in the vertical, we use integrated atmospheric reflectivity, transmissivity, absorptivity, and relative humidity for the atmospheric column. This assumption restricts the radiative convective transfer in the model.

Net solar heating in the water column is given as

$$Q_{SW_o} = Q_S \left\{ (1 - A_c) \left[T_r \, (1 - \alpha) / \left(1 - \alpha R_f\right) \right] + A_c \left[T_r^c \, (1 - \alpha) / \left(1 - \alpha R_f^c\right) \right] \right\}. \quad (4)$$

ii. Sensible and latent heat. Sensible heat (Q_{SH}) and latent heat (Q_{LHE}) fluxes are parameterized using traditional aerodynamic bulk formulae. At the surface, sensible heat flux is given by,

$$Q_{SH} = \rho_a C_h C p_a U \, (T_w - T_a), \quad (5)$$

where, C_h is the transfer coefficient for temperature and U is velocity at 10 m above the ocean surface. The subscripts "w" and "a" refer to the ocean surface and the air boundary level, respectively.

Latent heat released due to evaporation at the surface is given by

$$Q_{LHE} = \rho_a L_v C_{DE} U \, (q_w - q_a), \quad (6)$$

where L_v is latent heat of evaporation, C_{DE} is the transfer coefficient for humidity, and q is specific humidity. Latent heat is a function of saturation vapor pressure, which in turn is a function of the surface temperature. Following Hartmann (1994)'s simplification approach for latent heat (readers may refer to section 4.6 in Hartmann 1994 for a more detailed derivation) gives

$$Q_{LHE} = \rho_a L_v C_{DE} U \left[q_w^* \, (1 - RH) + RH \left. \frac{\partial q_w^*}{\partial T} \right|_{T_w} (T_w - T_a) \right], \quad (7)$$

where RH is relative humidity ($0 < RH < 1$) and q_w^* is the saturation vapor-mixing ratio at the ocean surface.Because Q_{LHE} is a positive quantity, $T_w > T_a$ always holds true. Although RH is a function of temperature, we shall assume RH to be constant (∼0.85), as any change due to temperature fluctuations is minimal. Note that, using the Clasius–Clapeyron relationship, the saturation vapor pressure is expressed as $e_s = e_0 e^{\left[\left(\frac{L_v}{R_v}\right)\left(\frac{1}{T_0} - \frac{1}{T_w}\right)\right]}$, where e_s is surface vapor pressure, e_0 is a reference vapor pressure, T_0 is a reference temperature, and R_v is the gas constant.

By definition, saturation vapor pressure is given by $q_w^* = \epsilon e_s / P_a$, where ϵ is a constant obtained from the ratio of R_d/R_v, R_d is the dry air constant, and P_a is surface pressure. Defining the Bowen ratio (Be) as $\left(Cp_a/L_v\right)\left(dq_w^*/dT_w\right)^{-1}$ and using the above expression for q_w^*, Eq. (7) can be simplified to

$$Q_{LHE} = \rho_a L_v C_{DE} U \left[q_w^* (1 - RH) + \frac{RH}{Be} \frac{Cp_a}{L_v} (T_w - T_a) \right], \tag{8}$$

iii. Surface and planetary long-wave radiation. Long-wave radiation emitted by the ocean surface can either be absorbed by the atmosphere or escape into space. We used the Fanning and Weaver 1996 parameterization. Upward long-wave radiation emitted by the ocean surface is absorbed by greenhouse gasses in the atmosphere and is reemitted back to the ocean surface. Hence, net long-wave radiation at the ocean surface (I_s) is

$$I_s = \varepsilon_w \sigma T_w^4 - \varepsilon_a \sigma T_a^4, \tag{9}$$

where ε is emissivity and σ is the Stefan–Boltzmann constant. The subscripts "w" and "a" refer to the ocean surface and the atmosphere.

Outgoing long-wave radiation is parameterized as a function of surface temperature (T_a), height mean relative humidity $\left(\overline{RH}\right)$ for clear and cloudy sky conditions, and radiative forcing due to changes in atmospheric CO_2 concentration (e.g., Thompson and Warren 1982; Weaver et al. 2001). Thus, planetary long-wave emission is given by

$$Q_{PLW} = R_1 - A_c R_2, \tag{10}$$

where

$$\begin{aligned}
R_1 &= a_0 + a_1 T_a + a_2 T_a^2 + a_3 T_a^3 - \Delta F \, ln \left(\frac{C(t)}{C_0} \right), \\
R_2 &= R_1 \left(T_a, \overline{RH}\right) - R_1 \left(T_c, \overline{RH}\right) + n_0 + n_1 (T_a - T_c) + n_2 (T_a - T_c)^2 \\
&\quad + n_3 (T_a - T_c) \left[\left((T_a - T_c) + n_4 \left(\overline{RH} + n_5 \right) \right) \right], \\
a_0 &= m_{00} + m_{10} \overline{RH} + m_{20} \overline{RH}^2, \; a_1 = m_{01} + m_{11} \overline{RH} + m_{21} \overline{RH}^2, \\
a_2 &= m_{02} + m_{12} \overline{RH} + m_{22} \overline{RH}^2, \text{ and } a_3 = m_{03} + m_{13} \overline{RH} + m_{23} \overline{RH}^2
\end{aligned}$$

where T_c is cloud top temperature, $C\,(t)$ is atmospheric CO_2 concentration, C_0 is present day value of CO_2 (350 ppm), and $\Delta F = 5.77\ Wm^{-2}$ is a constant radiative forcing of 4 Wm^{-2} for a doubling of CO_2. Readers may refer to Table 3 and Table 4 of Thompson and Warren (1982) for constants used. Eq. (10), therefore, simplifies to

$$Q_{PLW} = A_0 + A_1 T_a + A_2 T_a^2 + A_3 T_a^3, \tag{11}$$

where,

$$A_0 = a_0 - \Delta F\, ln\left(\frac{C\,(t)}{C_0}\right) + A_c\left(a_1 T_c + a_1 T_c^2 + a_3 T_c^3\right) - A_c\left(n_0 - n_0 T_c + n_2 T_c^2\right)$$
$$- A_c n_3\left(\overline{RH} + n_5\right)\left(T_c^2 - n_4 T_c\right),$$
$$A_1 = (1 - A_c)\, a_1 - A_c\,(n_1 - 2n_2 T_c) - A_c n_3\left(\overline{RH} + n_5\right)(2T_c - n_4),$$
$$A_2 = (1 - A_c)\, a_2 - A_c n_2 - A_c n_3\left(\overline{RH} + n_5\right), \quad \textit{and} \quad A_3 = (1 - A_c)\, a_3.$$

3. Exact solution to the "*Aqua Planet*"

We have Eqs. (1) and (2) to solve for unknown T_w and T_a, where T_w and T_a are the independent variables of this nonlinear algebraic system. In order to solve this system analytically, we, first, investigate the steady state solution (i.e., $d/dt \to 0$). Then, we add Eqs. (1) and (2) and substitute Eqs. (3)–(11) to obtain a simple analytical cubic expression for the atmosphere.

$$A_3 \overline{T}_a^3 + A_2 \overline{T}_a^2 + A_1 \overline{T}_a + A_0 - \left(Q_{SW_o} + Q_{SW_a}\right) = 0, \tag{12}$$

where "bar" denotes the mean steady state solution. Eq. (12) has three possible roots, but we will only consider real physical solutions. We do not show the possible three roots to the Eq. (12), but reader may refer to basic algebra books for the general solution (e.g., Cardano's method). Once we have the solution for $\overline{T}_a$, we then substitute to Eq. (2) to obtain the solution for $\overline{T}_w$. Because the saturation vapor pressure $\left(q_w^*\right)$ is nonlinear (see Section 2b), we must linearize q_w^* around a known temperature $(\hat{T}_w)$. An iterative solution—satisfying $error = \left|\overline{T}_w - \hat{T}_w\right| \approx 0$—is performed to derive an exact solution, where the known temperature $(\hat{T}_w)$ satisfies the condition $\left|\left(\overline{T}_w - \hat{T}_w\right)/\overline{T}_w\right| \ll 1$. The linearization of q_w^* can be found in Appendix B. Substituting Eqs. (B3) and (B4), the linearization of q_w^*, into Eq. (2), we obtain an algebraic equation for water temperature $\left(\overline{T}_w\right)$,

$$\varepsilon_w \sigma \overline{T}_w^4 + \left[\rho_a C_h C p_a U\left(1 + \frac{C_{DE}}{C_h}\frac{RH}{Be\left(\hat{T}_w\right)}\right) + \frac{\rho_a L_v^2 C_{DE} U\,(1 - RH)\, q_w^*\left(\hat{T}_w\right)}{R_v \hat{T}_w^2}\right]\overline{T}_w$$
$$- \varepsilon_a \sigma \overline{T}_a^4 - \rho_a C_h C p_a U\left(1 + \frac{C_{DE}}{C_h}\frac{RH}{Be\left(\hat{T}_w\right)}\right)\overline{T}_a - Q_{SW_o}$$
$$+ \rho_a L_v C_{DE} U\,(1 - RH)\, q_w^*\left(\hat{T}_w\right)\left[1 - \frac{L_v}{R_v \hat{T}_w}\right] = 0 \tag{13}$$

Although Eq. (13) has four roots, we only consider real positive solutions for the ocean. For mean global climate parameters, we evaluated Eqs. (12) and (13) to obtain model-predicted average global temperatures for the surface ocean $\left(\overline{T}_w\right)$ and atmosphere $\left(\overline{T}_a\right)$.

4. Results and discussion

a. Mean condition

Solutions derived from Eqs. (12) and (13) are presented below for present-day climate parameters. To complete the discussion, later we discuss the climate feedbacks due to changes in solar constant, cloud cover, and CO_2 concentration. Model-predicted warming/cooling due to feedbacks is compared with the recent IPCC results. Theoretically predicted mean oceanic $(\overline{T}_w)$ and atmospheric $(\overline{T}_a)$ temperatures are tested against the real observations for validation of the model physics. Zonal mean present-day climate parameters used for our analytical solution are $Be \sim 0.3$, $\rho_w = 1025\,kgm^{-3}$, $\rho_a = 1.25\,kgm^{-3}$, $C_h = 0.0009$, $Cp_w = 4000\,Jkg^{-1}K^{-1}$, $Cp_a = 1030\,Jkg^{-1}K^{-1}$, $\varepsilon_a = 0.84$, $T_0 = 0^0C$, $\varepsilon_w = 0.96$ $\sigma = 5.67e(-8)\,Wm^{-2}K^{-4}$, $RH = 0.85$, $L_v = 2.5e6\,Jkg^{-1}$, $R_v = 461\,JK^{-1}kg^{-1}$, $C_{DE} = 0.00135$, $e_0 = 611\,kPa$, $\epsilon = 0.622$, $U = 5\,ms^{-1}$, $P = 1.013e5\,Pa$, $A_b = 0.1967$, $R_f = 0.0651$, $A_c = 0.64$, $\alpha = 0.1$, $A_b^c = 0.1821$, and $R_f^c = 0.2962$.

Considering only real positive solutions Eqs. (12) and (13) we get $\overline{T}_a = 287.37\,K$ and $\overline{T}_w = 291.06\,K$, respectively. Thus, the model-predicted mean ocean is *3.69 K* warmer than the model-predicted mean atmosphere above it. Our results show a good agreement with the observed, using global meteorological network and satellites, global mean surface temperature where $\overline{T}_{obs} = 288\,K$ (Kramm and Dlugi 2011). Although the observed surface temperature contains the contribution from the land mass, we assume that the contribution is small on a global scale because more than 70% of the ocean surface is capable of storing heat compared with the land. However, our model-predicted offset contradicts Dietrich (1963)'s solution, where he showed the temperature offset as 0.8°C. Although his study was based on detailed measurements acquired in 1938 that included the seasonal variation in the forcing, our steady state solution ignores the seasonality in the signal. The solution for a modelled cloud-free atmosphere, $A_c = 0$, gives *304.99 K* and *303.43 K* for the ocean $(\overline{T}_w)$ and atmosphere $(\overline{T}_a)$, respectively, which agrees with the planetary radiative equilibrium solution derived using a simple greenhouse model (e.g., section 6.4.3 in Petty 2006).

Our model is limited in its ability to compute the planetary radiative equilibrium temperature for no atmosphere, because the parameterization used for planetary long-wave radiation is empirical and therefore includes the atmosphere in its constants. Note that, assuming black-body emission by the Earth's surface, planetary equilibrium temperature for no atmosphere is defined as $T_E = [Q_s\,(1 - \alpha_E)/\varepsilon_E\sigma]^{1/4}$, where, $Q_s = \frac{1360}{4}\,Wm^{-2}$, $\alpha_E = 0.3$, and $\varepsilon_E = 1$.

b. Climate sensitivity and the feedbacks

The analytical solution to our conceptual model is sensitive to selected climate parameters. Therefore, to add to the modeled climate variability discussion, we studied the modeled climate feedbacks to changes in solar constant, CO_2 concentration, and cloud cover. Thus, the climate forcing parameters change over a range and resulting temperature offset

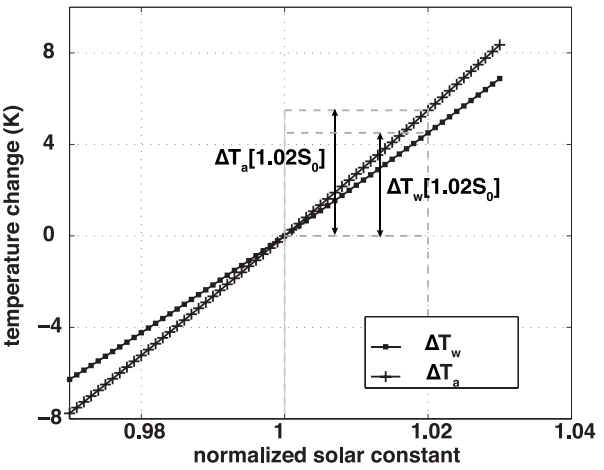

Figure 2. Change in temperature of the Surface Ocean and atmosphere with respect to a normalized solar constant for a *cloudy sky*. S_0 is the solar constant. The normalization is achieved by dividing the solar constant by the present day solar constant ($S_0 = 1360\ Wm^{-2}$). A 2% increase in the solar constant is equivalent to a doubling of CO_2 in the atmosphere. Warming due to a 2% increase in the solar constant is shown by the vertical arrows. For a cloudy sky, a 2% increase in the solar constant results in a *4.5042 K* and *5.4914 K* warming in the surface ocean and atmosphere, respectively.

is calculated. It is important to note that the expected warming may not be precise due to dominant feedbacks from various other parameters at such extremes. The IPCC Fifth Assessment Report (*AR5*) stated that "there is *high confidence* that equilibrium climate sensitivity (ECS) is *extremely unlikely* less than 1 K and *medium confidence* that the ECS is *likely* between 1.5 K and 4.5 K and *very unlikely* greater than 6 K."

i. Solar constant. A change in the solar constant implies a change in incoming solar radiation, which is derived by multiplying the solar constant ($S_0 = 1360\ Wm^{-2}$) by a constant factor. A 2% increase in solar radiation is equivalent to a doubling of the atmospheric CO_2 concentration (Shell and Somerville 2005). We set the CO_2 concentration $[C\ (t)]$ in the atmosphere to the reference CO_2 concentration (C_0) and, thus, the variability in the radiative forcing term in the outgoing long-wave radiation is zero $\left[\Delta F\ ln\left(\frac{C(t)}{C_0}\right) \approx 0\right]$. Hence, any model-predicted solution variability is solely due to a change in incoming radiation. Figure 2 illustrates the model-predicted variability in temperature offset ($\overline{\Delta T}_a\ and\ \overline{\Delta T}_w$) of the "*Aqua Planet*" to the changes in normalized solar constant. For a cloudy sky, a 2% increase in solar constant results in a warming of 4.5 K and 5.5 K in the modeled surface of the ocean $\left(\overline{\Delta T}_w\right)$ and atmosphere $\left(\overline{\Delta T}_a\right)$, respectively. Although our conceptual model surface warming lies within the limits given in IPCC AR5, the sensitivity for a 2% increase in solar radiation lies above the IPCC AR5 medium confidence. The deference in estimates perhaps is due to our one-layer atmospheric model lacking the lapse rate to change following

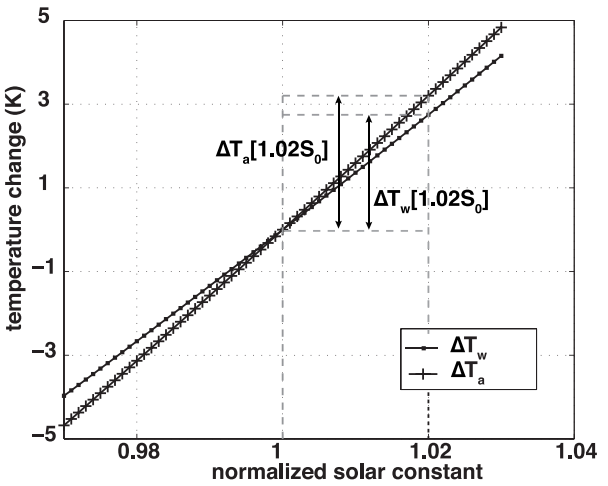

Figure 3. Change in temperature of the modeled Surface Ocean and atmosphere with respect to a normalized solar constant for a *clear sky*. S_0 is the solar constant. The normalization is achieved by dividing the solar constant by the present day solar constant ($S_0 = 1360\ Wm^{-2}$). A 2% increase in the solar constant is equivalent to a doubling of CO_2 in the atmosphere. Warming due to a 2% increase in the solar constant is shown by the vertical arrows. For a clouds-free sky, a 2% increase in the solar constant causes a 3.2 K and 2.7 K warming in the atmosphere and ocean, respectively.

moist adiabat. For a cloud-free sky, a 2% increase in solar constant gives a 3.2-K and 2.7-K warming in the model atmosphere and ocean, respectively (Fig. 3). In this scenario, our conceptual model's surface warming for a cloud free sky is within the IPCC AR5 medium confidence.

ii. Cloud amount. Figure 4 shows the variability in model prediction of surface temperatures in both the ocean and atmosphere for a varying cloud cover. We see that an increase in cloud cover decreases the surface temperature while increasing the ocean–atmosphere temperature difference (Fig. 5). Thus, cloud radiative effect leads to a strong ocean–atmosphere temperature offset at the surface. Figure 6 illustrates the evolution of surface temperature change (ocean and atmosphere) with respect to normalized cloud cover. A 20% increase in cloud cover results in roughly a 6°C and 8°C cooling in the ocean and atmosphere, respectively.

iii. CO_2 concentration. Setting the incoming radiation to a constant (i.e., solar constant is fixed), we shall examine the evolution of surface temperature change in the ocean and atmosphere with respect to a changing CO_2 concentration (Eq. 10). The resultant warming (Fig. 7) due to a doubling of CO_2 is 3.5 K and 4.4 K in the surface of the ocean and atmosphere, respectively. The above results show a good agreement with the IPCC AR5 assessment.

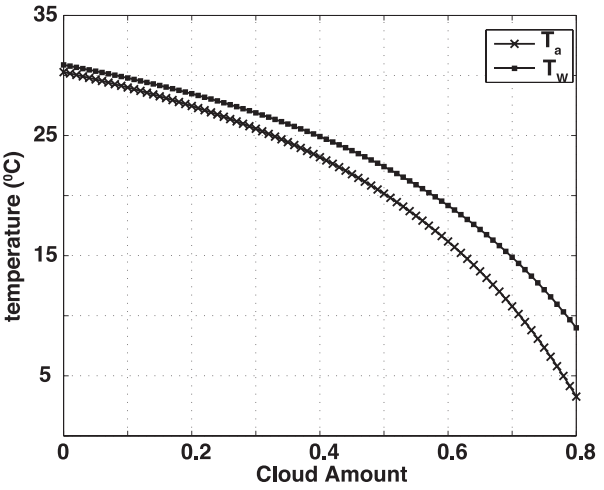

Figure 4. The evolution of surface temperature in both the ocean and atmosphere for changing cloud cover. It is shown that an increase in cloud cover decreases the surface temperatures in both the ocean and atmosphere.

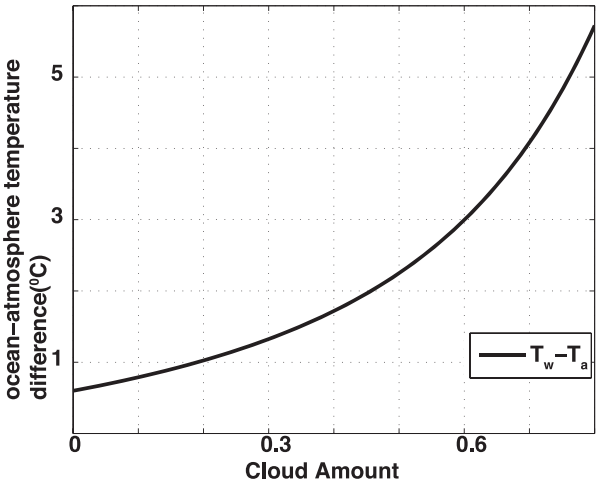

Figure 5. The evolution of air–sea temperature difference for varying cloud cover. Although an increase in cloud cover decreases individual surface temperatures in both the ocean and atmosphere (Fig. 4), it also increases the air–sea temperature offset.

c. Perturbation to the mean solution

For simplicity, we shall reparameterize the complex outgoing long-wave radiation into a simpler form. Assuming gray-body emission, we use Fanning and Weaver (1996)'s parameterization for planetary long-wave emission. Hence, we get

$$Q_{PLW} = \varepsilon_P \sigma T_a^4, \tag{14}$$

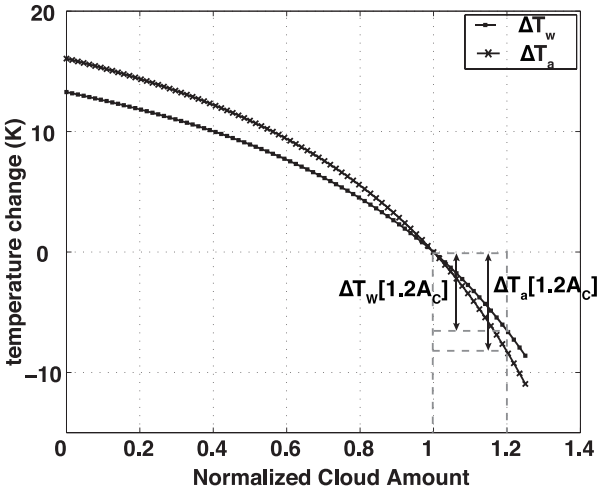

Figure 6. Evolution of surface temperature change (ocean and atmosphere) to a normalized cloud cover. A 20% increase in cloud cover results in roughly a 6°C and 8°C *cooling* in the ocean and atmosphere, respectively. The vertical arrows denote temperature change corresponding to a 20% increase in cloud cover. A_c is cloud cover.

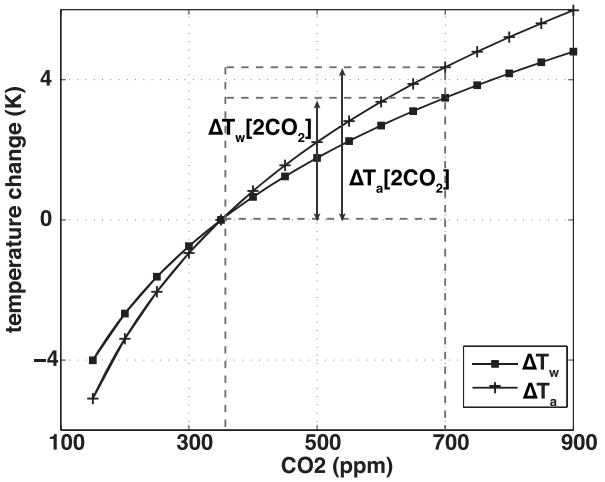

Figure 7. Evolution of surface temperature (ocean and atmosphere) to changes in CO_2 concentration in the atmosphere. The resultant warming due to a doubling of CO_2 is 3.4632 K and 4.3911 K in the Surface Ocean and atmosphere, respectively.

where ε_P is planetary emissivity. Planetary emissivity will be obtained from a balance between net solar radiation and the outgoing black-body radiation, where $\varepsilon_P = Q_s/\sigma\overline{T}_a^4$.

Perturbation of temperatures around the mean solution can be defined as

$$T_a = \overline{T}_a + T_a' \quad and \tag{15}$$

$$T_w = \overline{T}_w + T'_w, \tag{16}$$

where the "overbar" denotes a time mean and "prime" denotes a small temporal perturbation. Using Eqs. (15) and (16), we linearize Eqs. (1)–(9) and (14) assuming $\left|\left(\overline{T}_J - T'_J\right)/\overline{T}_J\right| \ll 1$, where, subscript "$J$" can be "$w$" (ocean) or "$a$" (atmosphere). See Appendix C for the linearization. We will build a simple perturbed climate model (anomaly model) for the "*Aqua Planet*" given in Eqs. (1) and (2) using Eqs. (C1)–(C6), ignoring products of anomalies, which are assumed to be small; anomalous heat content in the atmosphere is derived as

$$\begin{aligned}\rho_a H_a Cp_a \frac{\partial T'_a}{\partial t} = {} & Q'_{SW_a} + \rho_a C_h Cp_a U\left(T'_w - T'_a\right) + \overline{Q}_{LHE}\frac{L_v}{R_v \overline{T}_w^2} T'_w \\ & + \rho_a C_h Cp_a U \frac{RH}{Be\left(\overline{T}_w\right)}\left(1 + \frac{L_v}{R_v \overline{T}_w^2}\right)\left(T'_w - T'_a\right) \\ & + 4\varepsilon_w \sigma \overline{T}_w^3 T'_w - 4\varepsilon_a \sigma \overline{T}_a^3 T'_a - 4\varepsilon_p \sigma \overline{T}_a^3 T'_a. \end{aligned} \tag{17}$$

Eq. (17) can be further simplified to

$$\frac{\partial T'_a}{\partial t} = a_0 + \frac{a_1}{\rho_a H_a Cp_a} T'_w - \frac{(a_2 + a_3)}{\rho_a H_a Cp_a} T'_a, \tag{18}$$

where

$$\begin{aligned} a_0 &= \frac{Q'_{SW_a}}{\rho_a H_a Cp_a}, \\ a_1 &= \rho_a C_h Cp_a U\left(1 + \frac{RH}{Be\left(\overline{T}_w\right)}\right) + \overline{Q}_{LHE}\frac{L_v}{R_v \overline{T}_w^2} + 4\varepsilon_w \sigma \overline{T}_w^3, \\ a_2 &= \rho_a C_h Cp_a U\left(1 + \frac{RH}{Be\left(\overline{T}_w\right)}\right) + 4\varepsilon_a \sigma \overline{T}_a^3, \quad \text{and} \\ a_1 &= 4\varepsilon_p \sigma \overline{T}_a^3. \end{aligned}$$

A similar analysis can be done for the oceanic heat balance given in Eq. (2), such that

$$\begin{aligned}\rho_w H_w Cp_w \frac{\partial T'_w}{\partial t} = {} & Q'_{SW_o} - \rho_a C_h Cp_a U\left(T'_w - T'_a\right) - \overline{Q}_{LHE}\frac{L_v}{R_v \overline{T}_w^2} T'_w \\ & - \rho_a C_h Cp_a U \frac{RH}{Be\left(\overline{T}_w\right)}\left(1 + \frac{L_v}{R_v \overline{T}_w^2}\right)\left(T'_w - T'_a\right) \\ & + 4\varepsilon_w \sigma \overline{T}_w^3 T'_w - 4\varepsilon_a \sigma \overline{T}_a^3 T'_a. \end{aligned} \tag{19}$$

Eq. (19) simplifies to

$$\frac{\partial T'_w}{\partial t} = c_0 - \frac{a_1}{\rho_w H_w C p_w} T'_w - \frac{a_2}{\rho_w H_w C p_w} T'_a, \tag{20}$$

where, $c_0 = \frac{Q'_{SW_o}}{\rho_w H_w C p_w}$.

The matrix form of Eqs. (18) and (20) is

$$\frac{\partial}{\partial t}\begin{bmatrix} T'_a \\ T'_w \end{bmatrix} = \begin{bmatrix} a_0 \\ c_0 \end{bmatrix} + \begin{bmatrix} -\frac{(a_2+a_3)}{\rho_a H_a C p_a} & \frac{a_1}{\rho_a H_a C p_a} \\ -\frac{a_2}{\rho_w H_w C p_w} & -\frac{a_1}{\rho_a H_a C p_a} \end{bmatrix} \begin{bmatrix} T'_a \\ T'_w \end{bmatrix} \tag{21}$$

The above equation is equivalent to $\vec{X}' = A\vec{X} + \vec{f}(t)$, where

$$A = \begin{bmatrix} -\frac{(a_2+a_3)}{\rho_a H_a C p_a} & \frac{a_1}{\rho_a H_a C p_a} \\ -\frac{a_2}{\rho_w H_w C p_w} & -\frac{a_1}{\rho_a H_a C p_a} \end{bmatrix}, \quad \vec{X} = \begin{bmatrix} T'_a \\ T'_w \end{bmatrix} \quad \text{and} \quad \vec{f}(t) = \begin{bmatrix} a_0 \\ c_0 \end{bmatrix}.$$

By definition the general solution is $\vec{X}(t) = M(t)M(0)^{-1}\vec{X}(0) + \int_t M(t)M(s)^{-1} f(s)ds$, where $M(t) = \left[e^{\lambda_1 t}\vec{v}_1\ e^{\lambda_2 t}\vec{v}_2\right]$ such that λ_1 *and* λ_2 refer to eigenvalues of the homogeneous system and $\vec{v}_1$ and $\vec{v}_2$ are then the corresponding eigenvectors. Substituting present-day climate parameters given in section 4a, the obtained eigenvalues and eigenvectors are $\lambda_1 = -0.21x10^{-5}$, $\lambda_2 = -8x10^{-8}$, $\vec{v}_1 = \begin{bmatrix} 1 \\ -0.023 \end{bmatrix}$ and $\vec{v}_2 = \begin{bmatrix} 1 \\ 0.816 \end{bmatrix}$. The solution to the homogenous system is $X_h = C_1 e^{\lambda_1 t}\begin{bmatrix} 1 \\ -0.023 \end{bmatrix} + C_2 e^{\lambda_2 t}\begin{bmatrix} 1 \\ 0.816 \end{bmatrix}$, where C_1 and C_2 are constants derived from initial conditions and the subscript "h" refers to the homogenous solution. As time goes to infinity (i.e., $t \to \infty$), the magnitude of $X(t)$ decreases to zero, and as time goes to zero (i.e., $t \to 0$) $X(t)$ reaches a fixed point (i.e., $d/dt \to 0$) given by an initial condition. The phase portrait for this homogenous system shows a stable system explained above (Fig. 8). Solutions obtained for a nonhomogenous system (Fig. 9), by including temporal variations of insolation, reveal the magnitude of oscillations in air temperature anomalies is greater than those obtained in the ocean. A phase shift in the oscillations (a lag in the ocean) is caused by thermal inertia of the ocean.

d. Regional applications

To illuminate the importance of various regional dynamical processes, such as evaporative cooling, we formed a simple index that compared regional air–sea temperature difference with the global offset. Thus, we applied our conceptual model to marginal seas (e.g., Caspian Sea, Dead Sea, Red Sea, Black Sea, and Mediterranean Sea), the Gulf of Mexico, the equator (10 S–10 N), the subtropics (10 N–40 N), and the northern higher latitudes (40 N–60 N). Although temperature offsets obtained are generally close to observed values, we caution against taking individual temperatures in each medium for certain regions at face value. As an example, the temperature we derived from the "*Aqua Planet*" solution may not be true for

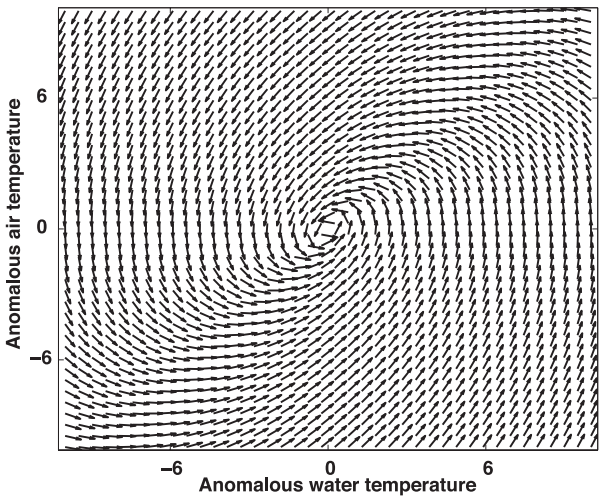

Figure 8. The phase portrait for the homogenous system, derived from a temporal perturbation of the mean solution of the "*Aqua Planet*". It shows a stable system.

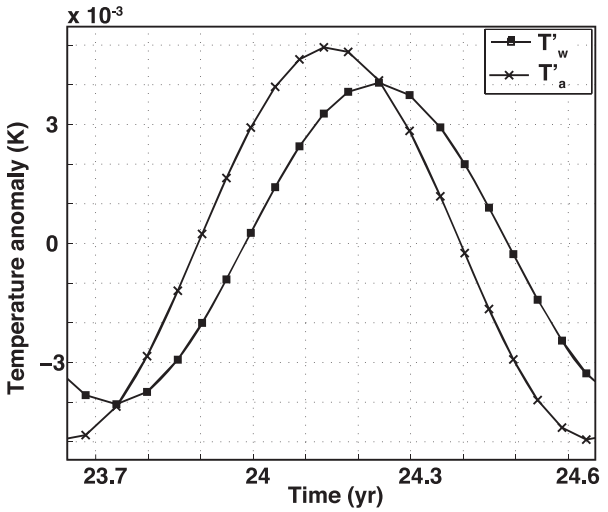

Figure 9. The solution obtained for a nonhomogenous system, by including temporal variation of insolation. The magnitude of the oscillation amplitudes of atmospheric temperature anomaly is greater to those found in the ocean. A phase shift in the oscillations (specifically a lag in the ocean) is due to the high thermal inertia of water compared with air.

the tropics due to the absence of lateral and land–sea heat transfer processes in our model. However, estimated temperatures obtained for marginal seas are in good agreement with those observed in the ocean and atmosphere. To understand the local evaporative cooling, we derived an index in which we normalize the regional offset with global temperature

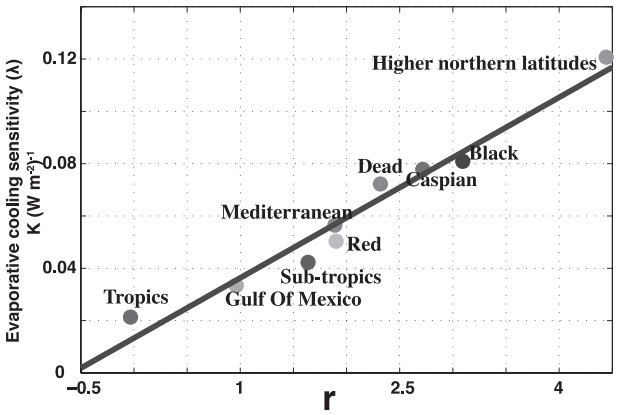

Figure 10. Application of the idealized *"Aqua Planet"* model to local regions (e.g., Caspian Sea, Dead Sea, Red Sea, Black Sea, and Mediterranean Sea, Gulf of Mexico, equator (10S–10N), subtropics (10N–40N), and northern higher latitudes (40N–60N)). A linear fit is shown as a bold black line. For a fixed relative humidity, increasing sensitivity of evaporative cooling increases surface evaporation, which in turn increases air–sea temperature offsets.

offset ($r = \psi/\overline{\psi}$, where, $\psi = T_w - T_a$). The $\overline{\psi}$ denotes the global mean. For fixed RH, in which the latent heat flux is proportional to the air–sea temperature offset, one may argue that the higher the ratio, the higher the evaporative cooling. We can further elaborate on this idea by explicitly incorporating latent heat into the ratio r. Thus, we will determine latent heat change with respect to the air–sea temperature offset. Differentiating Eq. (8) with respect to ψ gives

$$\frac{\partial Q_{LHE}}{\partial \psi} = Q_{LHE}\frac{L_v}{R_v T_w^2} + \rho_a C_{DE} L_v U q_s^* \frac{L_v}{R_v T_w^2}\left(1 - \frac{2\psi}{T_w}\right). \tag{22}$$

We define an evaporative cooling sensitivity parameter $\lambda = \left(\frac{1}{\overline{\psi}}\frac{\partial Q_{LHE}}{\partial r}\right)^{-1}$, where the "bar" denotes the mean global air–sea temperature offset obtained in section 4a for a cloud free atmosphere. In order to calculate the air–sea temperature offset for marginal seas, we use the Clouds and the Earth's Radiant Energy System (CERES) climatological shortwave flux data for different seas. For fixed RH, Figure 10 shows the rate at which the evaporative cooling sensitivity parameter (λ) increases for an increasing air–sea temperature offset. We can relate this idea to Ben-Sasson, Brenner, and Paldor (2009), who showed that maximum evaporation rate occurs during winter and minimum evaporation in summer. In winter, the air–sea temperature offset is positive where the evaporation is maximum due to atmospheric instability. The opposite occurs during summer. This means that, for higher air–sea temperature offsets, we would expect higher evaporative cooling. In cases where ψ is negative, the index λ is still a positive and greater than unity, indicating that the ocean is cooler than the atmosphere above it.

5. Summary and conclusion

A one-dimensional conceptual box model coupling the nonlinear ocean and atmosphere has been developed to theoretically determine air–sea temperature differences. The significance of this simple model lies in its analytical solution. Our model was able to steady state mean temperatures for the modeled ocean surface and atmosphere above it. Nonlinearity made the system of heat equations unsolvable analytically. Although a numerical solution is possible, we sought for an analytical solution because low-order models are best in capturing important thermodynamic processes setting the global climate. Thus, a simple scheme of iterative solution was applied to remove the nonlinearity in this complex thermodynamic system by assuming a known temperature and using the Taylor expansion method. Results obtained for the global climate show good agreement with observations.

The use of our model was demonstrated through a series of analyses. Temporal perturbation of the mean global solution obtained for "*Aqua Planet*" was used to determine the stability of the system, showing a stable system. Although the mean ocean is warmer than the mean atmosphere above it, atmospheric anomaly is greater in magnitude than those found in the ocean. In shorter time scales, high thermal inertia of the ocean causes a lag in response time for anomalous fluctuations compared with those in the atmosphere. Climate feedbacks due to incoming radiation, cloud cover, and CO_2 content were discussed. The warming we obtained may not be accurate due to dominant responses from other parameters at such extremes. As an example, the warming obtained for a 2% increase in solar radiation for a cloudy sky, which lies above the IPCC AR5 medium confidence, is possibly due to (1) large positive vertical water vapor feedback (from planetary long-wave radiation) and (2) a lack of negative lapse rate feedback to balance the shortwave radiation's positive feedback.

To complete the discussion, we applied our simple model to marginal seas (e.g., Black Sea, Caspian Sea, Red Sea, Mediterranean Sea, Red Sea, and Dead Sea), the tropics (10 S–10 N), the subtropics (10 N–40 N), and the northern higher latitudes (40 N–60 N). Our model solutions for enclosed seas approximate observations reasonably well. The evaporative cooling sensitivity parameter we derived illustrates that increases in the ratio of global-to-local air–sea temperature offset leads to increases in evaporative cooling and, therefore, an increase in the sensitivity to evaporative cooling.

APPENDIX A

LIST OF SYMBOLS AND ABBREVIATIONS–*AQUA PLANET* MODEL

SST	Sea surface temperature
COADS	Comprehensive Ocean-Atmosphere Data Set
ECMFW	European Centre for Medium-range Weather Forecasts
GCM	General circulation model
IPCC	Intergovernmental Panel on Climate Change
CERES	Clouds and the Earth's Radiant Energy System
T_a	Model atmospheric surface temperature

T_w	Model sea surface temperature
ρ_a	Atmospheric density (∼constant)
H_a	A constant scale height
Cp_a	Atmospheric specific heat capacity
Q_{SW_a}	Absorbed atmospheric short-wave radiation
Q_{SH}	Surface sensible heat
I_s	Net long-wave flux released at the surface to the atmosphere
Q_{PLW}	Net long-wave radiation escaping into space
Q_{LHE}	Latent heat
Q_{SW_o}	Absorbed oceanic short-wave radiation
α	Surface albedo
R_f	Reflectivity
A_b	Absorptivity
T_r	Transmissivity of the atmosphere
A_c	Cloud cover
Q_S	Average global incoming solar radiation at the top of the atmosphere
Q_{SH}	Sensible heat
C_h	Transfer coefficient for temperature
U	Velocity at 10 m
L_v	Latent heat of evaporation
C_{DE}	Transfer coefficient for humidity
q_w, q_a	Specific humidity, where subscripts "w" and "a" refer to the ocean surface and air at the boundary level, respectively.
RH	Relative humidity
q_w^*	The saturation vapor-mixing ratio at the ocean surface
e_s	Surface vapor pressure
e_0	Reference vapor pressure
T_0	Reference temperature
R_v	Gas constant
ϵ	Constant obtained from the ratio of R_d/R_v, R_d is the dry air constant
R_d	Dry air constant
Be	Bowen ratio
$\varepsilon_w, \varepsilon_a$	Emissivity of the sea surface and atmosphere, respectively
σ	Stefan–Boltzmann constant
T_c	Cloud top temperature
$C(t)$	Atmospheric CO_2 concentration
C_0	Present day value of CO_2 (350 ppm)
$\Delta F = 5.77\ Wm^{-2}$	A constant radiative forcing of 4 Wm^{-2} for a doubling of CO_2
ε_P	Planetary emissivity
ρ_w	Mean seawater density
H_w	Mixed ocean depth

Cp_w	Ocean specific heat capacity
P	Surface pressure
ψ	The regional modeled ocean–atmosphere temperature difference
$\overline{\psi}$	The predicted global *Aqua Planet* ocean–atmosphere temperature difference
r	The evaporative cooling ratio ($\psi/\overline{\psi}$)
λ	The evaporative cooling sensitivity

APPENDIX B
LINEARIZATION OF SATURATION VAPOR PRESSURE AND THE BOWEN RATIO-MEAN MODEL

Assume a known temperature $\left(\hat{T}_w\right)$, where $\left|\overline{T}_w - \hat{T}_w/\overline{T}_w\right| \ll 1$. The saturation mixing ratio $\left(q_w^*\right)$ can be approximated with a first-order Taylor series.

$$\overline{q}_w^*\left(\overline{T}_w\right) = q_w^*\left(\hat{T}_w\right) + \left.\frac{dq_w^*}{dT}\right|_{\hat{T}_w}\left(\overline{T}_w - \hat{T}_w\right) \tag{B1}$$

Using the Clasius–Clapeyron relationship (section 2b), saturation vapor pressure is expressed as $e_s = e_0 e^{\left[\frac{L_v}{R_v}\left(\frac{1}{T_0}-\frac{1}{T_w}\right)\right]}$. Note that saturation vapor pressure is $q_w^* = \epsilon^{e_s}/P$. Hence, the Bowen ratio (Be) can be expressed as $\frac{Cp_a}{L_v}\left(\frac{dq_w^*}{dT}\right)^{-1}$, which means $\frac{dq_w^*}{dT} = \frac{\epsilon}{P}\frac{de_s}{dT}$. This gives

$$\frac{dq_w^*}{dT} = \frac{L_v}{R_v\hat{T}_w^2}q_w^*\left(\overline{T}_w\right). \tag{B2}$$

Substitution of Eq. (B2) into Eq. (B1) yields

$$q_w^*\left(\overline{T}_w\right) = q_w^*\left(\hat{T}_w\right)\left[1 + \frac{L_v}{R_v\hat{T}_w^2}\left(\overline{T}_w - \hat{T}_w\right)\right]. \tag{B3}$$

Thus, the Bowen ratio becomes

$$Be\left(\overline{T}_w\right) = \frac{Cp_a}{L_v}\left(\left.\frac{dq_w^*}{dT}\right|_{\hat{T}_w}\right)^{-1} = \frac{Cp_a}{L_v}\left(\frac{q_w^*\left(\hat{T}_w\right)L_v}{R_v\hat{T}_w^2}\right)^{-1}. \tag{B4}$$

APPENDIX C
PERTURBATION OF HEATING COMPONENTS

C.1 Perturbation of sensible and latent heat

Using the assumptions given in Eq. (15) and (16), the temperature-dependent saturation vapor pressure can be redefined as a function of the perturbation, $e_s = e_0 e^{\left[\frac{L_v}{R_v}\left(\frac{1}{T_0}-\frac{1}{\overline{T}_w}-\frac{T'_w}{T'^2_w}\right)\right]}$.

By definition, the saturation vapor-mixing ratio at the surface is $q_w^* = \epsilon^{e_s}/P$. Therefore, $\frac{dq_w^*}{dT} = \frac{\epsilon}{P}\frac{de_s}{dT} = -\frac{L_v}{R_v \overline{T}_w^2} q_w^*$.

Now, we shall use first order Taylor expansion—similar to Hartmann (1994)—for the saturation vapor-mixing ratio of air. This gives us $q_w^* = \overline{q}_w^* \left(1 + \frac{L_v}{R_v \overline{T}_w^2} T_w'\right)$, where $\overline{q}_w^*$ is the saturation vapor mixing ratio at temperature $\overline{T}_w$. The corresponding Bowen ratio can be defined as $\frac{1}{Be} = \frac{1}{Be(\overline{T}_w)} \left(1 + \frac{L_v}{R_v \overline{T}_w^2} T_w'\right)$, where $Be(\overline{T}_w)$ is the Bowen ratio at temperature $\overline{T}_w$. Using the linearized saturation mixing ratio and Bowen ratio, Eq. (8) transforms to

$$Q_{LHE} = \overline{Q}_{LHE} + Q_{LHE}\left(L_v/R_v \overline{T}_w^2\right) T_w' + \rho_a C_h C p_a U \left(C_{DE} RH/C_h Be(\overline{T}_w)\right)\left(T_w' - T_a'\right), \tag{C1}$$

where $\overline{Q}_{LHE}$ is the time mean of latent heat due to evaporation. Similarly, we shall compute the linearized sensible heat given in Eq. (2). We get

$$Q_{SH} = \overline{Q}_{SH} - \rho_a C_h C p_a U \left(T_w' - T_a'\right) \tag{C2}$$

where $\overline{Q}_{SH}$ is the time mean sensible heat released at the surface.

C.2 Perturbation of long-wave radiation

Likewise, we shall linearize both the surface long-wave radiation and the planetary long-wave radiation. Removing higher order perturbation terms (∼small), the expansion of $I_s = \overline{I}_s - \varepsilon_w \sigma \left(\overline{T}_w - T_w'\right)^4 - \varepsilon_a \sigma \left(\overline{T}_a - T_a'\right)^4$ gives

$$I_s = \overline{I}_s - 4\varepsilon_w \sigma \overline{T}_w^3 T_w' - 4\varepsilon_a \sigma \overline{T}_a^3 T_a' \tag{C3}$$

where $\overline{I}_s$ is the time mean net back radiation at the surface. The linearized planetary long-wave emission given in Eq. (14) transforms to

$$Q_{PLW} = \overline{Q}_{PLW} - 4\varepsilon_p \sigma \overline{T}_a^3 T_a', \tag{C4}$$

where $\overline{Q}_{PLW}$ is the average long-wave emission to space.

C.3 Perturbation of shortwave radiation

In the case of a temporal perturbation of the "Aqua Planet" model, an annual cycle for insolation is used—as was done in North and Coakley (1979)—to relax the constraint imposed by the mean condition in Eqs. (3) and (4). Therefore, contributions from seasonal variations in the ocean surface and atmospheric temperature fields will be included in the model. The seasonal solar radiation function is modeled as $Q_t = Q_s + |Q_0| \cos(2\pi t/yr)$,

where Q_0 is the amplitude of the seasonal variation and t is time. Thus, the absorbed radiation in both the ocean and atmosphere becomes

$$Q^t_{SW_o} = Q_t \left(A + T\alpha A / \left(1 - \alpha R\right)\right) \tag{C5}$$

and

$$Q^t_{SW_a} = Q_s \left(T(1 - \alpha) / \left(1 - \alpha R\right)\right). \tag{C6}$$

Acknowledgments. Girihagama acknowledges valuable discussion with Stephen Van Gorder regarding iterative solution. Dr. Cathrine Hancock is thanked for her valuable comments. This is contribution number 470 for the Geophysical Fluid Dynamics Institute at Florida State University. Lakshika Girihagama was partially supported by GFDI. The study was supported by NASA Doctoral Fellowship Grant NNG05GP65H, AGS Grant (1032403), LANL/IGPP Grant (1815), NSF (OCE-0752225, OCE-9911342, OCE-0545204, and OCE-0241036), BSF (2006296), and NASA (NNX07AL97G).

REFERENCES

Ben-Sasson, M., S. Brenner, and N. Paldor. 2009. Estimating air–sea heat fluxes in semienclosed basins: the case of the Gulf of Elat (Aqaba). J. Phys. Oceanogr., *39*, 185–202.

Bryan, K., S. Manabe, and R. C. Pacanowski. 1975. A global ocean-atmosphere climate model. Part II: the ocean circulation. J. Phys. Oceanogr., *5*, 30–46.

Bryan, K., S. Manabe, and M. Spelman. 1988. Interhemispheric asymmetry in the transient response of a coupled ocean-atmosphere model to a CO_2 forcing. *J. Phys. Oceanogr*., *18*, 851–867.

Budyko, M. I. 1969. The effect of solar radiation variations on the climate of the Earth. Tellus, *21*, 611–619. doi: 10.1111/j.2153-3490.1969.tb00466.x

Cubasch, U., K. Hasselmann, H. Hock, E. Maier-Reimer, U. Mikolajewicz, et al. 1992. Time-dependent greenhouse warming computations with a coupled ocean atmosphere model. *Climate Dyn. 8*, 55–69.

Dietrich, G. 1963. General oceanography, New York, Wiley, 588p.

Dines, W. H. 1917. The heat balance of the atmosphere. Q. J. R. Meteor. Soc., *43*, 151–158.

Fanning, A. F. and A. J. Weaver. 1996. An atmospheric energy-moisture balance model: climatology, interpentadal climate change, and coupling to an ocean general circulation model. J. Geophys. Res., *101*, 15111–15128. doi: 10.1029/96JD01017

Gates, W. L., Y. J. Han, and M. E. Schlesinger. 1985. The global climate simulated by a coupled atmosphere-ocean general circulation model, preliminary results, in *Coupled Ocean Atmosphere Models*. C. J. Nihoul, Ed., *Elsevier Oceanogr. Ser*., 40J., Elsevier, New York, 131–151.

Hartmann, D. L. 1994. Global Physical Climatology. Cambridge: Academic Press, 411 p.

Kara, A. B., H. E. Hurlburt, and W. Y. Loh. 2007. Which near–surface atmospheric variable drives air–sea temperature differences over the global ocean? J. Geophys. Res. Oceans, *112*, 5020. doi: 10.1029/2006JC003833

Kramm, G. and R. Dlugi. 2010. On the meaning of feedback parameter, transient climate response, and the greenhouse effect: basic considerations and the discussion of uncertainties. Open Atmos. Sci. J., *4*, 137–159. doi: 10.2174/1874282301004010137

Kramm, G. and R. Dlugi. 2011. Comments on the paper "A new basic 1-dimensional 1-layer model obtains excellent agreement with the observed Earth temperature" by Rainer Link and Horst-Joachim Lüdecke. arXiv preprint arXiv:1112.1135.

Link, R. and H. J. Lüdecke. 2011. A new basic 1-dimensional 1-layer model obtains excellent agreement with the observed Earth temperature. Int. J. Mod. Phys. C, *22*, 449–455. doi: 10.1142/S0129183111016361

Liu, W. T. 1988. Moisture and latent heat flux variabilities in the tropical Pacific derived from satellite data. J. Geophys. Res., *93*, 6749–6760. doi: 10.1029/JC093iC06p06749

Manabe, S., and K. Bryan. 1969. Climate calculations with a combined ocean-atmosphere model. J. Atmos. Sci., *26*, 786–89. doi: 10.1175/1520-0469(1969)026<0786:CCWACO>2.0.CO;2

Manabe, S., and R. J. Stouffer. 1988. Two stable equilibria of a coupled ocean-atmosphere model. *J. Climate*, *1*(9), 841–866.

Manabe, S., K. Bryan, and M. J. Spelman. 1975. A global ocean-atmosphere climate model. Part I. The atmospheric circulation. J. Phys. Oceanogr., *5*, 3–29. doi: 10.1175/1520-0485(1975)005<0003:AGOACM>2.0.CO;2

Manabe, S., Bryan, K., and M. J. Spelman. 1990. Transient response of a global ocean-atmosphere model to a doubling of atmospheric carbon dioxide. *J. Phys. Oceanogr*., *20*(5), 722–749.

Manabe, S., M. J. Spelman, and R. J. Stouffer. 1992. Transient responses of a coupled ocean-atmosphere model to gradual changes of atmospheric CO_2. Part II: Seasonal response. *J. Climate*, *5*(2), 105–126.

North, G. R. and K. Y. Kim. 2017. Energy Balance Climate Models. Hoboken: John Wiley and Sons. 392 p.

North, G. R. 1975. Analytical solution to a simple climate model with diffusive heat transport. J. Atmos. Sci., *32*, 1301–1307. doi: 10.1175/1520-0469(1975)032<1301:ASTASC>2.0.CO;2

North, G. R. and J. A. Coakley. 1979. Differences between seasonal and mean annual energy balance model calculations of climate and climate sensitivity. J. Atmos. Sci., *36*, 1189–1204.

Petty, G. W. 2006. A First Course in Atmospheric Radiation, 2nd ed. Madison: Sundog Publishing. 452 p.

Rasool, S. I., and S. H. Schneider, 1971. Atmospheric carbon dioxide and aerosols: Effects of large increases on global climate. *Science*, *173*, 138–141. doi: 10.1126/science.173.3992.138.

Schlesinger, M. E., W. L. Gates, Y. J. Han. 1985. The role of the ocean in CO_2-induced climate warming: Preliminary results from the OSU coupled atmospheric-ocean GCM, in *Coupled Ocean-Atmosphere Models*. J. C. J. Nihoul, Ed., Elsevier, New York, 447–478.

Sellers, W. D. 1969. A global climatic model based on the energy balance of the earth–atmosphere system. J. Appl. Meteorol., *8*, 392–400. doi: 10.1175/1520-0450(1969)008<0392:AGCMBO>2.0.CO;2

Sellers, W. D. 1974. A reassessment of the effect of CO_2 variations on a simple global climatic model. *Journal of Applied Meteorology*, *13*(7), 831–833.

Shell, K. M. and R. C. J. Somerville. 2005. A generalized energy balance climate model with parameterized dynamics and diabatic heating. J. Clim., *18*, 1753–1772. doi: 10.1175/JCLI3373.1

Singh, R., C. M. Kishtawal, and P. C. Joshi. 2005. Estimation of monthly mean air–sea temperature from satellite observations using genetic algorithm. Geophys. Res. Lett., *32*, L02807. doi: 10.1029/2004GL021531

Sperber, K. R., S. Hameed, W. L. Gates, and G. L. Potter. 1987. Southern Oscillation simulated in a global climate model. *Nature*, *329*, 140–142.

Thompson, S. L. and S. G. Warren. 1982. Parameterization of outgoing infrared radiation derived from detailed radiative calculations. J. Atmos. Sci., *39*, 2667–2680. doi: 10.1175/1520-0469(1982)039<2667:POOIRD>2.0.CO;2

Trenberth, K. E., J. T. Fasullo, and J. Kiehl. 2009. Earth's global energy budget. Bull. Amer. Meteor. Soc., *90*, 311–323. doi: 10.1175/2008BAMS2634.1

Wang, Z., R. M. Hu, L. A. Mysak, J. P. Blanchet, and J. Feng. 2004. A parametrization of solar energy disposition in the climate system. Atmos. Ocean, *42*, 113–125. doi: 10.3137/ao.420203

Weaver, A. J., M. Eby, E. C. Wiebe, C. M. Bitz, P. B. Duffy, T. L. Ewen, A. F. Fanning, et al. 2001. The UVic Earth System Climate Model: model description, climatology and application to past, present and future climates. Atmos. Ocean, *39*, 361–428. doi: 10.1080/07055900.2001.9649686

Received: *7 December 2015*; revised: *8 June 2018*.